Seasonal wind analysis in Limassol, Cyprus, using the ground-based Doppler LiDAR of the CARO National Facility

Konstantinos Chrysostomou*[a,b]; George Kotsias[a]; Patric Seifert[c]; Argyro Nisantzi[a,b]; Diofantos G. Hadjimitsis[a,b]; Rodanthi E. Mamouri[a,b]
[a]Eratosthenes Centre of Excellence, 82 Franklin Roosevelt, Limassol, Cyprus 3012; [b]Department of Civil Engineering and Geomatics, Cyprus University of Technology, 30 Archiepiskopou Kyprianou, Limassol, Cyprus 3036; [c] Leibniz Institute for Tropospheric Research (TROPOS), 15 Permoserstraße, Leipzig, Germany 04318;

*constantinos.chrysostomou@eratosthenes.org.cy; phone +35797617832; eratosthenes.org.cy

ABSTRACT

The study focused on utilizing, for the first time ever, the data of the Halo Photonics Streamline XR Doppler LiDAR (Snoopy), which is an active remote sensing instrument that since January 2023 has been operating at the National Facility of the Cyprus Atmospheric Remote-Sensing Observatory (CARO) located in Limassol, Cyprus. The data spanned two full years of observations, from February 2023 to January 2025, in order to analyze the average wind patterns over the city, with the aim of understanding the diurnal, as well as the monthly and seasonal variations in both the horizontal wind speed and direction. The research involved processing data collected at various times of the day and across different atmospheric heights to calculate the mean horizontal wind and to identify common or characteristic patterns in the behaviour of the wind across months or seasons. An important outcome of this procedure is that the behaviour of the wind of this region can be sufficiently described through its separation into two periods of six months: the warm one from May till October, and the cold one from November until the month of April. The study also highlights the influence that local topographical factors have on the observed wind patterns, as both the land and sea breezes present a diurnal cycle and constitute a key characteristic of the winds that affect the city.

Keywords: Wind, Doppler LiDAR, Planetary Boundary Layer, Meteorology, Cyprus, EMMENA region

1. INTRODUCTION

With the term atmosphere we call the layer of gases that usually surrounds a planet, mainly due to its strong field of gravity. Here on Earth, the atmosphere shields the planet from the - in many cases - hazardous and catastrophic cosmic radiation, and especially radiation coming from the Sun, mostly by filtering them, and therefore plays a crucial role in sustaining life. It is primarily composed by nitrogen (around 78%), and oxygen (approximately 20%), along with traces of other gases like carbon dioxide, methane, and water vapor, that not only act as protective shield for life on the planet, but also regulate temperature, make the weather patterns and water cycle possible, and influence the dynamics of the global climate [1]. As a consequence, understanding and monitoring the atmosphere is fundamental for weather prediction, climate impact evaluations, and preserving environmental health and human well-being.

Winds arise when variations in atmospheric pressure drive air from regions of higher pressure towards regions of lower pressure, with this pressure-gradient force being directly proportional to the strength of the pressure difference. At the same time as air accelerates under this force, the Earth's rotation causes the Coriolis effect, which deflects the wind to the right in the Northern Hemisphere and to the left in the Southern Hemisphere. The magnitude of the effect increases with increases in latitude and wind speed, becoming negligible at the equator but dominant at high latitudes, hence resulting in the development of large wind systems such as the trade winds, westerlies, and polar easterlies. Moreover, near the surface of the Earth, friction with topography and vegetational features disturbs the balance, slowing and deflecting airflow, whilst at altitudes within the planetary boundary layer, where friction's effects decay, winds approach geostrophic balance – where pressure-gradient and Coriolis forces become nearly equal – producing more steady and accelerated wind flows. [2]

Eleventh International Conference on Remote Sensing and Geoinformation of the Environment (RSCy2025), edited by Andreas Christofi, et al., Proc. of SPIE Vol. 13816 · © The Authors. Published under a Creative Commons Attribution CC-BY 4.0 License · doi: 10.1117/12.3073303

Planetary Boundary Layer or else PBL, is called the bottommost part of the atmosphere, which is strongly influenced by the Earth's surface through frictional effects and the rapid transfers of heat, momentum, and water vapor. These interactions are critical to modulating the distribution of aerosols, trace gases, and contaminants from the land to the upper atmosphere, and thus acting as important factors in analyzing regional weather patterns, quality of air, and climate model studies, hence affecting our everyday lives [3, 4]. This layer can extent up to several kilometers above the ground surface [4]. Moreover, after long Sun exposure, and especially in times of extreme ground heating, the air masses above the ground start to heat up, becoming less dense, and therefore ascend, making colder and more dense air parcels to be convectively displaced downwards, taking the place of the warmer masses, marking the formation of the Convective Boundary Layer (CBL) - or else Mixing Layer (ML) [5]. These upward and downward movements of the air cause turbulent eddies inside the PBL, altering the behavior of the wind, and that's how pollutants, particulate matter, and aerosols disperse in the atmosphere, while the height of this convective sublayer can reach up to hundreds of meters above the ground, depending on the extent of the eddies. Thus, during the hours of convection, different wind behaviour and patters are expected.

Limassol, the region of interest of this study, is a coastal and the southernmost city of the island of Cyprus, located in the southeastern part of Europe, in the region of Levantine. It is therefore directly influenced by the Mediterranean Sea, which also defines its climate as according to the Köppen–Geiger Classification scheme, Limassol lies into the Csa category, characterized as Mediterranean with hot and arid summers, and with mild and wet winters [6]. Also, as coastal city, frequent sea and land breezes are observed, arising due to the strong temperature differences between land and sea, with air masses usually flowing from the sea towards the land during the day, marking the sea breezes, contributing to the ventilation of the city and the reduction of the pollutants, whilst the opposite happens during the night, where land breezes are observed.

This study aims to investigate the monthly and seasonal horizontal wind patterns influencing the coastal city of Limassol, Cyprus - a region where meteorological conditions are strongly modulated by complex topographical factors, and which is situated within the climatically sensitive area of the Eastern Mediterranean. Despite its vulnerability to climate variability, the region remains understudied in terms of climatological, meteorological, and atmospheric studies, but now, for the first time ever in Cyprus, a comprehensive wind analysis can be made possible through the use of a high-resolution, two-year-long dataset obtained from a Doppler lidar system. These data permit a detailed characterization of the region's wind climatology and intra-annual variability, offering new insights into the interactions between atmospheric circulation, local topography, and seasonal weather patterns in the area.

The paper is structured as follows: Section 2 describes the dataset and the methodology that was followed in order to retrieve the information of the horizontal wind, and to make the monthly and seasonal analysis, whilst Section 3 presents the outcomes of the study and discusses the results. Lastly, Section 4 of Conclusions summarizes and gives the overall findings of this study.

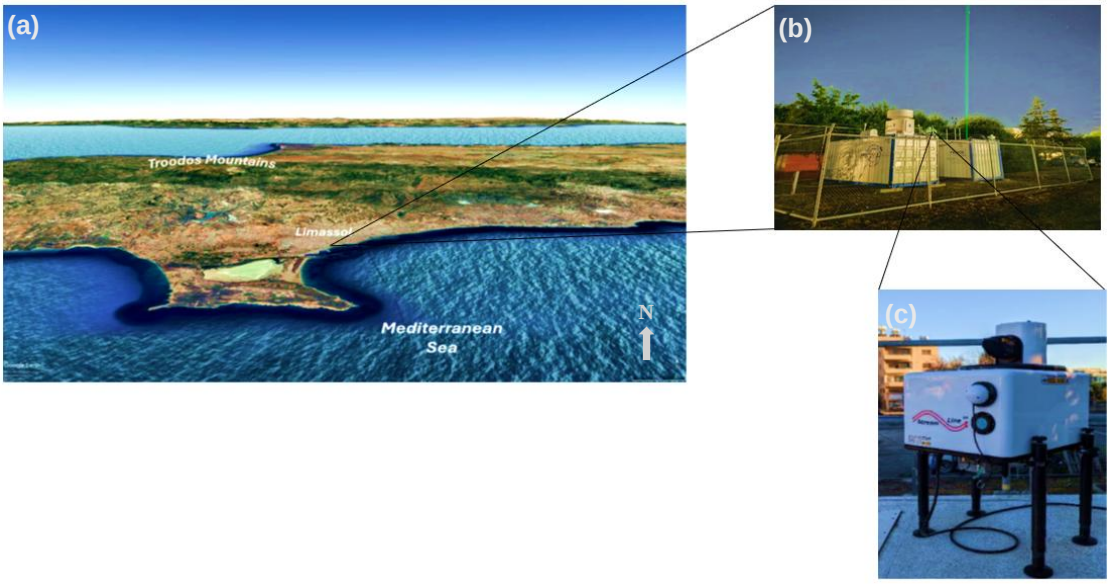

Figure 1: (a) Satellite view of the southern coast of Cyprus, depicting the location of Limassol. (b) Night shot of the CARO facility. (c) The Snoopy Doppler Lidar that was used for the analysis.

2. DATA AND METHODOLOGY

2.1 Snoopy Doppler LiDAR Measurements

The National Facility of the Cyprus Atmospheric Remote Sensing Observatory (CARO) is a ground-based remote sensing station located in Limassol (34.677076° N, 33.037608° E), at an altitude of approximately 10 m above mean sea level, and at a distance of merely 850 meters away from the coastline. It operates under the surveillance of ERATOSTHENES Centre of Excellence, offering complete insights into atmospheric dynamics, supporting atmospheric monitoring, and further advancing atmospheric and climate research, as special instruments for both aerosol and cloud monitoring function there. Since late January 2023, the station has been equipped with the Halo Photonics Streamline XR Doppler Lidar (Snoopy), an instrument that specializes in capturing the three-dimensional motion of the air, as it is able to operate in two modes; the stare one that retrieves the information of the vertical wind's updrafts or downdrafts, and the VAD (Velocity-Azimuth Display) one that is able to provide the information of the horizontal wind speed and direction. Figure 1b portrays the CARO field site, while Figure 1c shows a closer look of the Snoopy Doppler Lidar at the site.

In contrast to traditional instruments that measure the wind, the Doppler lidar by emitting electromagnetic radiation at the near-infrared part of the spectrum, can capture in high detail the variations of the wind over time and altitude, making it invaluable for studying phenomena such as vertical wind shear, turbulence, boundary layer dynamics, wind flow patterns or local wind effects, while its ability to work continuously, including both day and night and in all types of weather, ensures consistent and valuable data collection, which supports both weather forecasting, atmospheric monitoring, and climatological research, as can be seen from the studies of [7] and [8]. Table 1 provides some of the technical parameters of operation of the Doppler Lidar at the CARO site.

In a day of full operation without any disruptions, measurements of the vertical wind were obtained every 2 seconds, in which velocities of positive sign were recorded when scatterers moved away from the laser's direction, contrariwise to the negative sign that occurred when the scatterers moved towards the instrument. Positive velocities correspond, therefore, to wind updrafts and negative ones to downdrafts. However, every 15 minutes of vertically pointing measurements, the instrument stopped its vertical operation and started performing the VAD scans, resulting in 97 measurements of the horizontal wind speed and direction in a day of uninterrupted operation. To achieve this, the laser beam changed its elevation angle from 90°, at which the vertical measurements were obtained, to 60°. During this scan, the instrument rotated its laser beam at the fixed elevation angle allowing it to measure wind from various azimuthal angles, thus building a 360° view of the wind's radial velocity behavior at different heights, with these measurements being used to calculate the horizontal wind speed and direction by fitting them onto a sinusoidal model [9, 10]. As a result of the simulation is the retrieval of the u and v components of the wind, which represent the zonal (eastward) and the meridional (northward) components, respectively, out of which the speed of the horizontal wind as well as its direction can be obtained, after using the following respective trigonometric formulae [9]:

$$V_{HOR} = \sqrt{u^2 + v^2}\,, \tag{1}$$

$$\theta = \arctan\left(\frac{v}{u}\right) \tag{2}$$

Table 1. Operational details of the Doppler Lidar

Parameters	Values
Wavelength	1540 nm
Laser Energy	0.99 μJ
Lens Diameter	10 cm
Beam Divergence	33 μrad
Pulse Repetition Frequency	15 kHz
Range Resolution	48 m
Number of Pulses per Ray	50000
Number of Samples per Gate	1500
Pulse Duration	0.2 μs

2.2 Statistical analysis

2.2.1 Extraction of the Monthly and Seasonal average wind

For the calculation of the average speed of the horizontal wind of each month, the recorded wind between February 2023 and January 2025 was retrieved, using the parameters of time, height, and advection (horizontal) speed. Time was measured in UTC hours, height in meters, and advection speed was measured in ms^{-1}. The data were categorized according to the month that they were obtained, leading to a number of 730 data in total, due to a malfunction of the instrument on February 17th, 2023, which was the only month having one less day without any recorded data.

For each month, the wind speed measurements were averaged across all the available days at matching time and height bins, excluding any NaN values. The temporal dimension was divided into 24 one-hour bins, so in each time bin 4 or 5 measurements that were taken during that one-hour interval were first averaged, while the height dimension kept its original resolution of approximately 48 meters for each bin. As a result, the average wind speed of each month was represented by a 250 x 24 matrix, with rows corresponding to height levels and columns to the hours of the day. The exact same procedure was followed in order for the monthly average wind direction per hour and per height to be calculated. The monthly plots are shown in Figure 2 and Figure 3 for the mean horizontal speed and direction respectively, but up until the height of 3.5 km which was selected due to increased measurement noise and uncertainty at higher altitudes, most likely caused by the reduced aerosol concentrations and signal attenuation that yielded to lower SNR values.

The same methodology was applied to calculate the seasonal averages of horizontal wind speed and direction. Each day was assigned to a season based on the conventional classification, so that winter consisted of the months of December, January, and February; spring consisted of the months March, April, and May; summer consisted of the months of June, July, and August; and autumn consisted of the months of September, October, and November. The number of days contributing to the seasonal averages was 180 for winter, 184 for spring, 184 for summer, and 182 for autumn. For each season, two 250 x 24 matrices were again generated: one for the mean wind speed and one for the mean wind direction. Figure 4 and Figure 5 illustrate the results from this process respectively for the average seasonal wind speed and direction.

To better enhance the interpretation of seasonal patterns and their differences, average wind speeds were further analyzed based on the time of the day. Specifically, for each height level an average wind speed value was calculated, according to if it was daytime or night-time for that season. For the season of winter daytime is defined, based on the median sunrise and sunset times, between the hours 04:50 and 15:00 UTC, for spring between 03:15 and 16:20 UTC, for summer between 02:45 and 17:00 UTC, whereas for autumn daytime is defined between 03:50 and 15:15 UTC. Figure 6 depicts the results of this procedure. Also, to better clarify the differences between day and night between each season the average wind speed, and in this case the average direction too, of each height bin at 12:00 and 24:00 UTC of each season were calculated. These hours were chosen, as around 12:00 UTC in Cyprus the Sun's influence is strong enough, because the Sun is near its maximum elevation angle for both the winter and summertime, in contrast to 24:00 UTC which was chosen as at that time the influence from the Sun has long gone, and hence the dynamics of the atmosphere have a very different behaviour than during the day. Thus, wind differences between day and night can be seen more easily. Figure 7a shows the results for the mean seasonal wind speed per height at 12:00 UTC, Figure 7b the same but at 24:00 UTC, whereas Figure 8 depicts the respective plots for the case of wind direction.

As a last step, the average semi-annual wind speed and wind direction was calculated, following the same procedure that was followed before for the calculation of the average wind speed and direction of every month and season. Two plots are the results of this procedure for the wind speed and two for the wind direction: one of each for the cold season and one of each for the warm one. The cold season consisted of the months from November to April, whereas the warm season of the months May to October, so data from 362 and 368 days were used for the cold and warm season, respectively. How each month was classified as cold or warm is explained in the presentation of the results and the discussion in section 0. The results of this process are revealed in Figure 9a and Figure 9b for the speed and in Figure 9c and Figure 9d for the direction.

3. RESULTS AND DISCUSSION

3.1 Statistics of Wind Speed

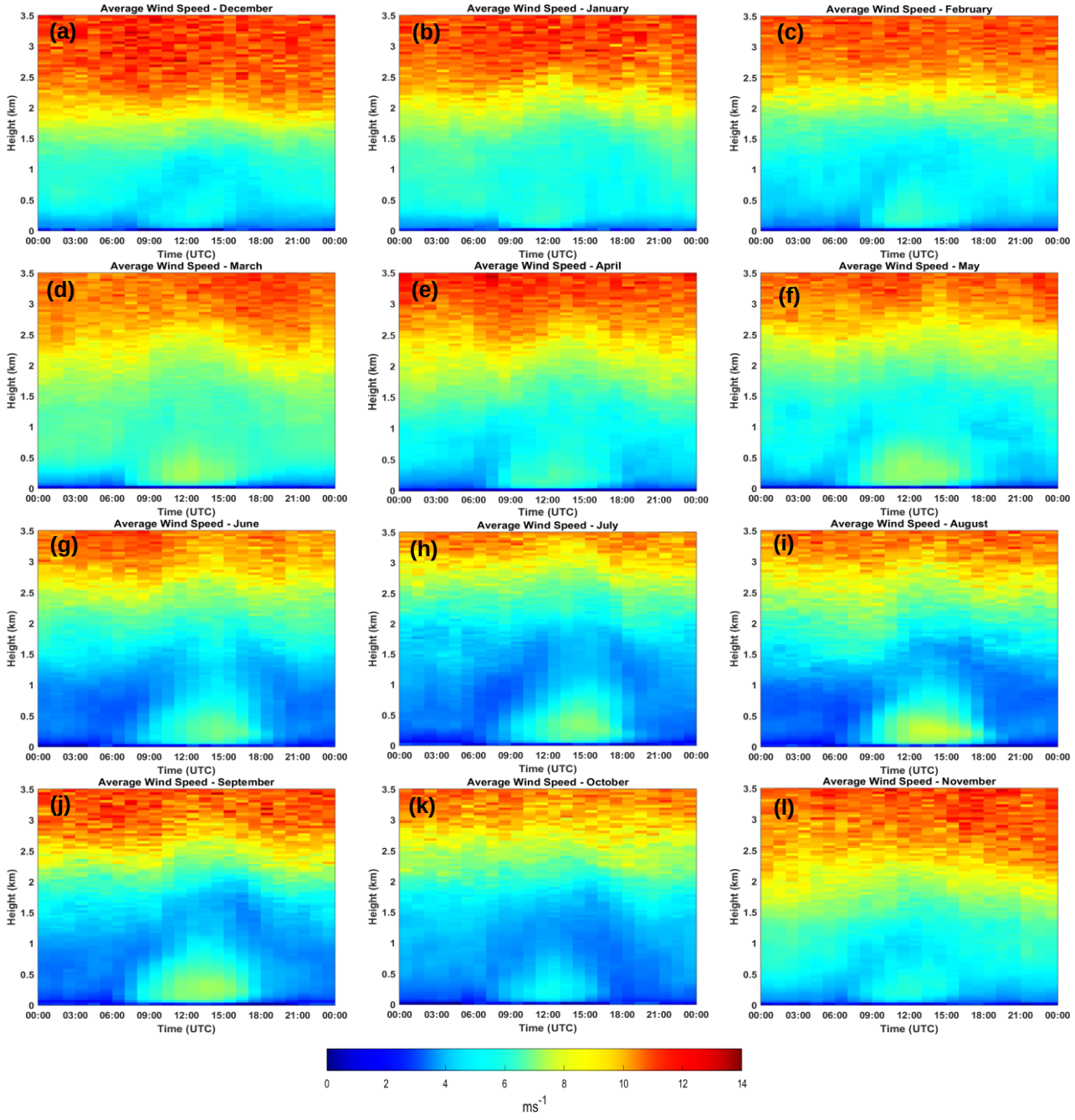

Figure 2(a-l): Time-height plots of the average wind speed of every month. Each color represents a wind speed value in ms-1 as shown in the color scale at the bottom of the figure.

The plots (Figure 2) of the monthly average wind speed present a consistent diurnal trend around the year with pronounced seasonal changes. Near-surface wind speeds (below 250 m) stay low throughout the night (below 4 ms^{-1}) but show a significant gain in the daytime, as the average horizontal wind speed usually exceeds 7 ms^{-1}. At mid-level altitudes

(between 500 to 1500 m), the daily wind speeds show a significant decrease before rising with the altitude. At high altitudes (above 2000 m), the wind speeds oftentimes exceed 9 ms^{-1} and can go as high as 14 ms^{-1}, depending on the season.

The time-height plots illustrated in Figure 2 exhibit the presence of two seasonal groups: the cold season from November to April and the warm period from May to October, as the months in these groups share a similar wind profile. This division highlights the influence of the seasonal temperature variations on the atmospheric wind dynamics, while this classification is in accordance with a recent study [11] that used 40-year-long ERA5-Land data and highlighted the presence of these two "seasons" for Cyprus. A key difference between these seasonal classes is marked by the strongly more reduced wind speeds noted between heights of 500 to approximately 1500 m during daytime in the warm months, coupled with the much more strengthened low-level winds (ranging from 0 to 500 m), which is most likely an indicator of increased vertical mixing within the mixing layer due to solar radiation. This process is most visible in June and least apparent in December, thus highlights the role of solar insolation. Comparably, the winter season (DJF) shows considerably high and uniform wind speeds throughout the vertical profile, with an average speed of over 6 ms^{-1} even in lower altitudes and up to stable speeds of 9-12 ms^{-1} at altitudes over 2000 m (see Figure 4a). By contrast, the summer months (JJA) shows weak nocturnal winds up to 1500 m and diurnal winds that can reach up to 9 ms^{-1} below 1000 m, along with a layered wind structure above, characterized by a mid-level lull followed by increasing speeds at higher altitudes. The seasonal transition periods of spring (March, April, May) and autumn (September, October, November) are remarkable. In March, April, and November (Figure 2d, Figure **2**e, Figure **2**l respectively), the atmospheric conditions most closely approximate those of winter with strong winds that exceed 10 ms^{-1} from lower altitudes (~1500 m) coupled with a weakly defined entrainment zone. May, September, and October (Figure 2f, Figure **2**j, Figure **2**k respectively) on the other hand, display more summer-like conditions with lower mid-level winds and increased wind dynamics above around 2500 m.

On average, it is a common feature across all the months that nocturnal winds close to the surface are in general low (less than 3 ms^{-1}) and calm conditions prevail, whilst during daytime the winds start to increase significantly, peaking in the months of summer and staying limited to around 6 ms^{-1} in the colder ones, while having shorter duration. Another notable characteristic are the strong winds (reddish colours on plots) that exhibit the upper altitudes in each one of the months, with the difference however that these winds occur at much lower heights during the cold season (see for example December - Figure 2a) in comparison to the warm season where strong winds start to build up at sometimes much higher altitudes (see the month of July - Figure 2h).

All of the aforementioned characteristics and behaviours of the average horizontal wind speed over Limassol can be seen concisely and coherently in the plots of the average seasonal wind, specifically for winter in Figure 4a, for spring in Figure 4b, for summer in Figure 4c, and lastly for the season of autumn in Figure 4d. These plots of each season serve as a good approximation for the expected wind of the months that constitute them, while the mean sunrise and sunset times are visible to highlight Sun's influence on wind dynamics.

Moreover, the differences between day and night-time seasonal winds per height can be seen in Figure 6(a-d), better facilitating the comparison between different months, seasons, and conditions (i.e., day or night). In these plots we can easily see that wind does not vary at all during the cold months of the winter, as almost the same wind speed is expected in both day and night for all the heights. This, however, changes as we move towards warmer months, culminating in the season of summer where the greatest difference between day and night is observed, with night-time winds being the weakest among all the seasons (< 4 ms^{-1}). In general, stronger winds are expected during the cold period (November to April), exceeding 8 ms^{-1} after 1.5 to 2 km of height in winter and spring, something which happens only after 2.5 km for summer and a little less than that for autumn. The average daytime wind speed of all seasons remains around 5 ms^{-1} (only in spring some stronger winds are expected) for the lower heights below 1km, whilst of key interest is the fact that above the convective heights (above the PBL), the expected wind speed increases linearly with the altitude in every season. Furthermore, during the hours of strong convection near the surface (see Figure **7**(a, b): Plots of the average seasonal wind speed per height for (a) 12:00 UTC, and (b) 24:00 UTC. The legend indicates which season each color represents.Figure 7a), the expected wind speed is greater than 5ms^{-1} across all seasons, peaking in spring (~ 7ms^{-1}) and then followed by summer, then autumn, and at last winter, all of them recording speeds close to 6 ms^{-1}. Once again, a decrease is obvious between 250 to 1000 meters, followed by a steady increase up to 3.5 km in all seasons. Compared to noon, midnight winds (Figure 7b) are much weaker and more uniform across seasons, increasing gradually with height. Notably, at altitudes above 1000 m, winter exhibits the strongest winds overall, while summer has the weakest, both during midday and midnight.

3.1 Statistics of Wind Direction

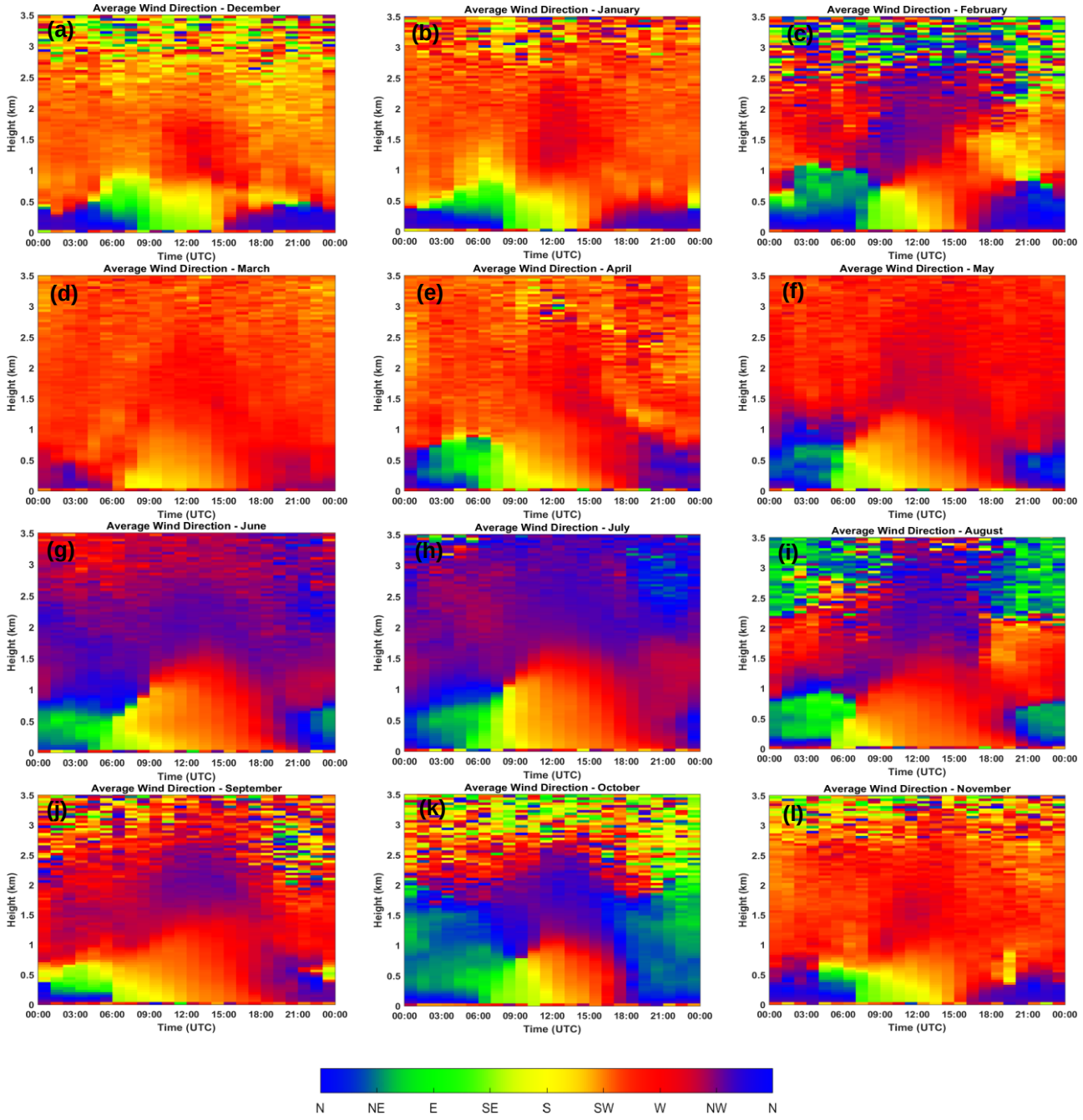

Figure 3(a-l): Time-height plots of the average monthly wind direction. Each color represents the direction of the wind as shown in the color scale at the bottom of the figure. Wind direction values of 0°/360° are displayed as North (N) and 90° as East (E).

Compared to wind speed, the monthly mean wind direction shows considerable variation, particularly at higher levels and seasonally during the summer months. While seasonal changes are represented by trends in wind speed, wind direction is more clearly defined for individual months beyond the first kilometre. Near the surface, however, a directional stability is apparent in all months. The dominant wind patterns during *winter* months (see Figure 3a-c and Figure 5a) often change from northerly (N) or north-westerly (NW) at night to south-easterly (SE), then to southerly (S), and finally to south-westerly (SW) during the daytime, to return to NW-N winds in the evening. At altitudinal zones ranging from 1000 to

2500 m, the prevailing wind patterns are generally from the southwest and west, with a significant dominance of NW winds noted during February. *Spring* months (Figure 3d-f), March, April, and May, show relatively stable directional patterns with no significant variations. Their night-time winds stayed mainly NW-N, but for April and May shifted during the day to eastern, southern, and then western near the surface, and only southern to western for March, while the winds above 1.5 km remained SW - W with some signs of NW throughout the day. This makes March the only month with no signs of easterly winds, among not just the months of spring, but among all the 12 months. The greatest directional variability, however, is found during *summer* months (Figure 3g-i). At heights under the influence of surface conditions, a clear diurnal pattern is found, with a clockwise shift in wind direction from north to southeast, south, southwest, west, and back to north. During convective daytime hours, especially above 1.5 km, winds are largely directed from north to northwest with a mixture of westerly to northerly winds during night-time for June and July, as opposed to the dominance of westerly winds between 1.5 to 2 km and easterlies between 2 and 3.5 km for August. The months of *autumn* (see Figure 3j-l) show patterns similar to those of summer; however, the SE-S-W phase shows a significant decrease in both duration and intensity. At high altitudes, the wind directions show noteworthy changes: September is dominated by the W-NW winds, October is influenced by E-SE, W, and N winds, and November is largely influenced by W-SW winds.

Above 2.5 km, for most months, wind direction appears inconsistent and varies from bin to bin. This likely results from lower aerosol concentrations at these altitudes, leading to weaker backscattering and noisier measurements. Notably, colder months exhibit more noise, something that is expected as the boundary layer doesn't extend to such high altitudes, and aerosols remain closer to the surface [10].

In general, a regular daily pattern of wind direction controlled by solar exposure is seen over most of the months, with a shift from easterly – south-easterly (ESE) to southerly (S) and then to south-westerly (SW) winds at noon. This pattern is the result of the effect of solar heating combined with boundary layer dynamics. Both the northerly to north-westerly winds prevailing during nighttime can be attributed to the *land breezes* influencing the Limassol city, and also the winds blowing predominantly from the southern direction during daytime are an evident signature of *sea breezes*.

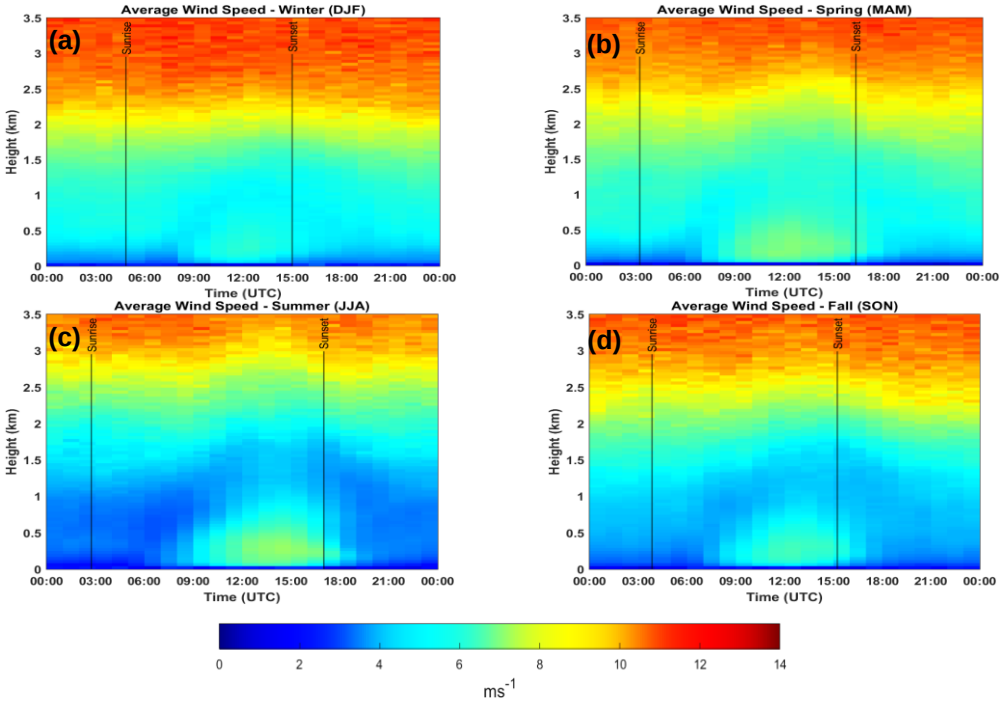

Figure 4(a-d): Time-height plots of the average seasonal wind speed. Each color represents the speed of the wind in ms-1, as shown in the color bar at the bottom of the figure. The black lines on each plot represent the mean sunrise and sunset time of each season, as inscribed on them.

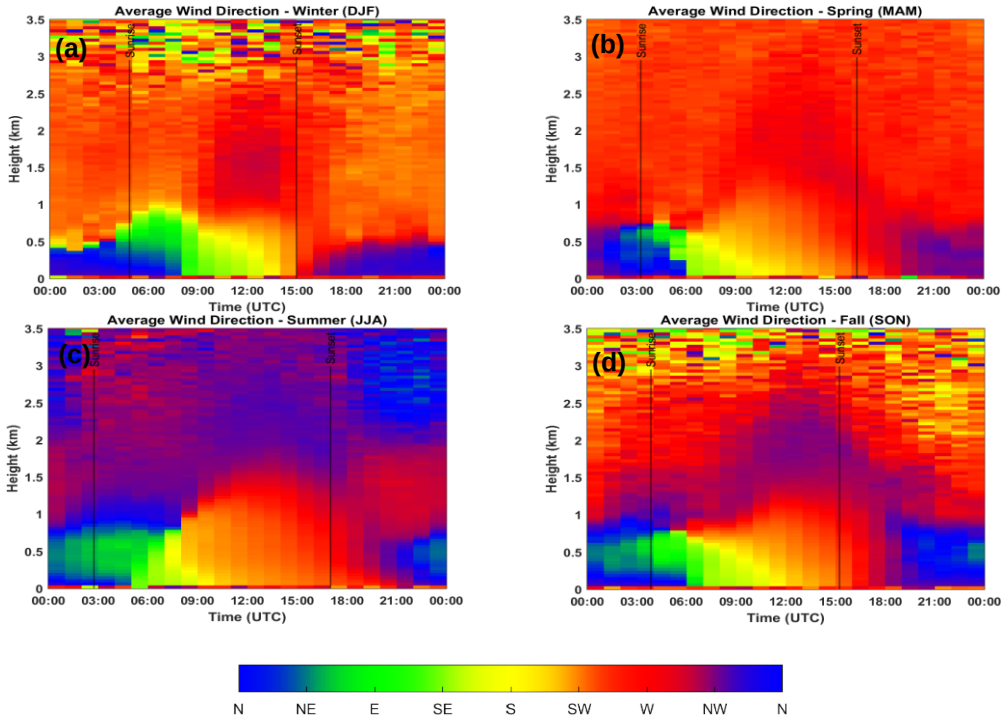

Figure 5(a-d): Time-height plots of the average seasonal wind direction. Each color represents the direction from which the wind blows, represented by the color bar at the bottom of the figure. North (N) represents directions from 0°/360° and East (E) from 90°. The black lines on each plot stand for the mean sunrise and sunset time of each season, as inscribed on them.

The plots in Figure 5, that present the results of the average seasonal wind direction, can again help to interpret the observed wind patterns above Limassol and also provide insight into the prevailing wind directions of the individual months within each season. It is easier to understand that the same directional pattern is observed at the lowermost heights across all months, with more exaggerated and pronounced directional layers during the warmer months. Likewise, above the first kilometres of the atmosphere, westerlies are seen mostly during the colder months (winter and spring, see Figure 5a and Figure 5b respectively), whereas north-westerly winds are expected during summer months (Figure 5c), and westerly to north-westerly winds in fall (Figure 5d).

Similarly, the plots in Figure 8 can facilitate the interpretation of the differences in wind direction between daytime and night at various altitudes, clearly highlighting the presence of sea and land breeze systems. That is, as at 12:00 UTC (Figure 8a) below 500 m, all the seasons experience winds between 135° and 225° (southerlies) shifting to W-NW as we move higher up. In contrast, the opposite happens during nighttime at 00:00 UTC (Figure 8b) where no southerly winds are expected. Instead, lower altitudes are dominated by northerly winds, indicative of land breezes, while higher altitudes generally show westerly flow – except in summer, where north-northwesterly (NNW) winds are more prevalent.

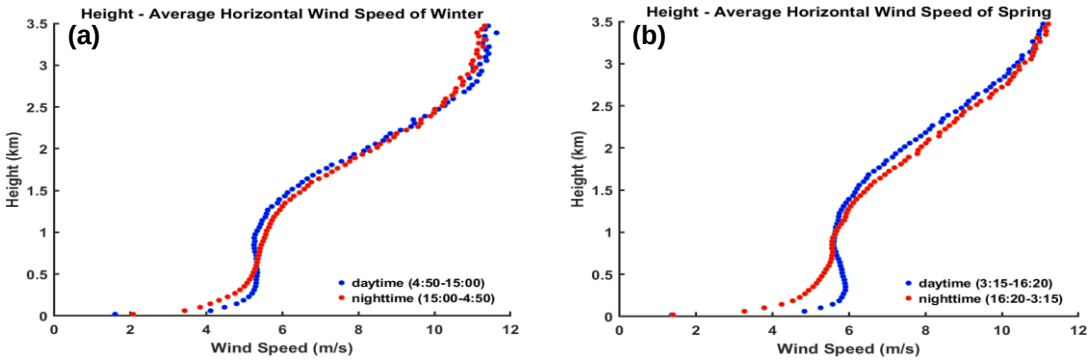

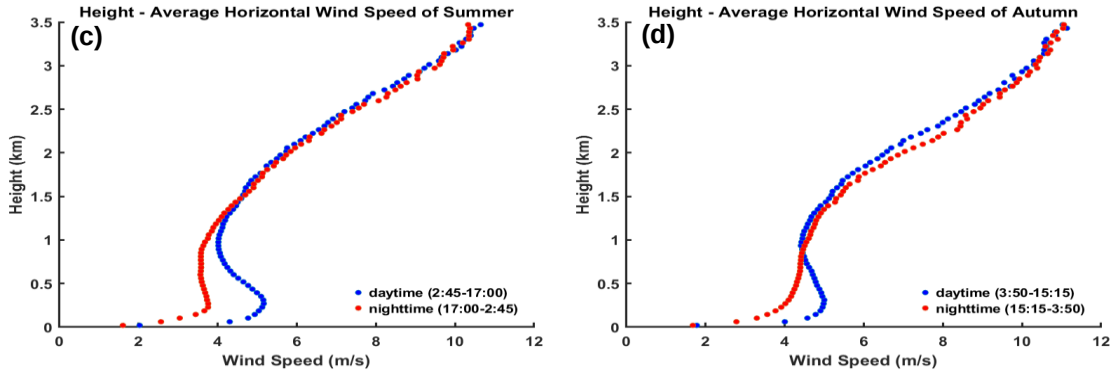

Figure 6(a-d): Plots of the average seasonal wind speed per height for different time periods of a day. The legend indicates what period each color represents. x-axis represents the average wind speed, whereas y-axis the height.

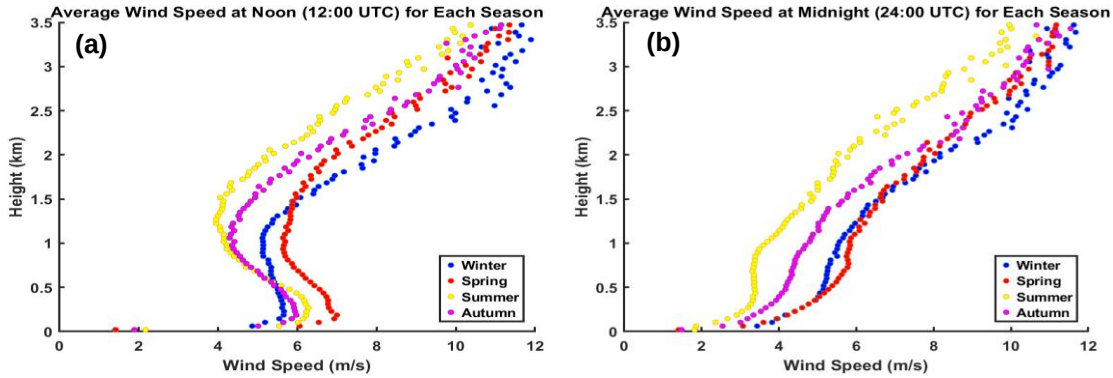

Figure 7(a, b): Plots of the average seasonal wind speed per height for (a) 12:00 UTC, and (b) 24:00 UTC. The legend indicates which season each color represents.

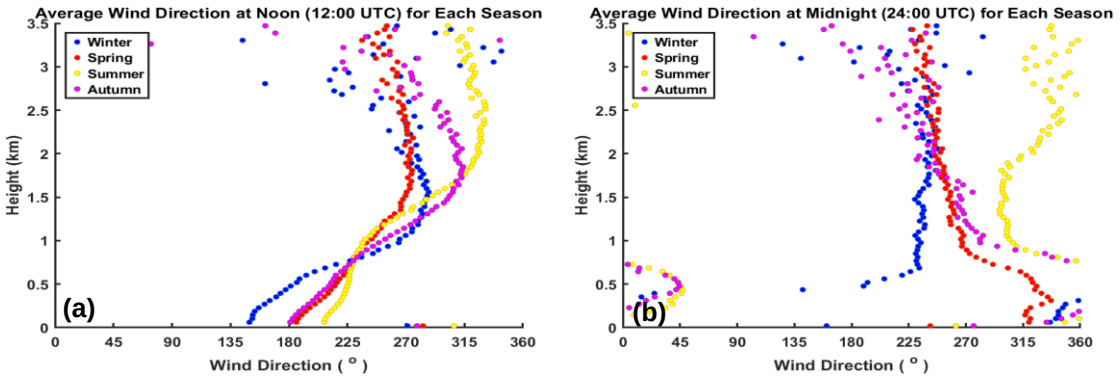

Figure 8(a,b): Plots of the average seasonal wind speed per height for (a) 12:00 UTC, and (b) 24:00 UTC. The legends indicate the season that each color represents. 0° and 360° represent the North, whereas 90° represent the East direction.

3.3 Semi-annual wind

As mentioned already, winds in Cyprus can be grouped into two categories: the cold one and the warm one. The plots in Figure 9 offer a clearer view of the wind patterns, as well as make more distinguishable the differences observed between cold and warm months. As seen, stronger winds are expected in general between the months of November to April (cold season) than between May and October (warm season).

In Figure 9(a-b) this statement can easily be seen, as strong winds (> 7 ms^{-1}) start from an altitude of about 1500 m in cold season, versus over 2 km in the warm season. The observed average wind speeds in the mixing layer, though, weren't

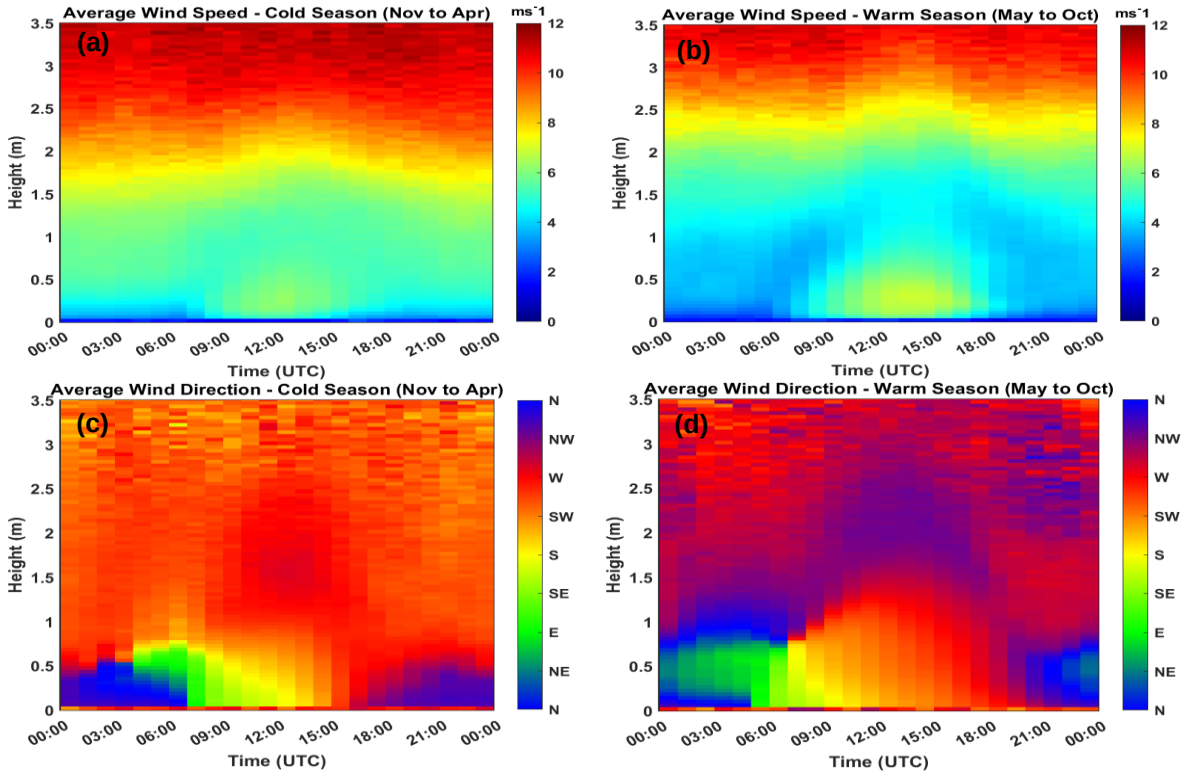

Figure 9(a-d): Time-height plots of the six-month averaging. Plots (a) and (b) represent the average wind speed for the cold and warm season, respectively. Next to them the color bar shows what speed each color represents. Plots (c) and (d) represent the average wind direction for the cold and warm season, respectively. Each color represents the direction from which the wind blows, as indicated in the color bar next to the plots.

much different between the two seasons, as in both ones they reach up to approximately 7 ms^{-1}. The extent of this layer, however, is what is different as it starts at around 08:00 and lasts until 17:00 UTC in the cold season, in contrast to the warm period where it spans between 07:00 and 20:00 UTC. On the other side, the decrease of the average wind speed above the convective layer during the warm season is much more noticeable than what it is during the cold one. The average wind speed between the months of November and April above the ML is somewhere between 5 and 6 ms^{-1}, contrariwise to the 3 to 4 ms^{-1} that are expected during the warm season.

Similar is the case for the average wind direction of the two six-month periods, as shown in Figure 9(c-d). First, the pattern that the wind direction follows just above the surface (under 250 m) is almost the same, as the change from north during the nighttime to east and southeast and then to south and to west-southwest during the daytime, occurs in both ones. The extent and the duration of the S-SE to S to WSW pattern is again different between the two seasons, in both time and height, matching the behavior of wind speed. In the cold season this pattern is observed between 07:00 and 17:00 UTC, up until 500 m of altitude, contrariwise to 05:00 and 19:00 UTC during the warm season, until heights of around 1500 m. Another noticeable difference is that above the ML, at altitudes between 1500 and 2500 m, the wind direction is mostly NW during the warm season whereas it is W-NW during the cold one, and also significant is the fact that variability of the direction between the months of May and October is greater, as it ranges between W and N, compared to WSW that is expected throughout the day during the cold season.

4. CONCLSUSIONS

The observed seasonal patterns reveal pronounced diurnal variations in wind speed and direction, with distinct characteristics detected between them. Some of the months and seasons, however, exhibited some obvious common patterns which led to their grouping and their distinction into two six-month periods: the warm one and the cold one. The warm season consists of the months between May and October, whereas the cold one between the months of November to April, something that has already been demonstrated before but never with wind data.

In addition, the analysis of the mean seasonal wind speed revealed that during the winter, high wind speeds prevail in both daytime and nighttime for altitudes even below 2000 m, with speeds reaching up to 8 ms^{-1} there and exceeding 12 ms^{-1} after 2500 m of altitude. In contrast, summer winds are generally weaker, especially during nighttime, where average speeds drop to 3–4 ms^{-1} for several heights above the ground surface and only after almost 3500 m exceed 12 ms^{-1}. Following on, the diurnal variations demonstrate a consistent increase in wind speed during daytime for heights close to the ground in every month, attributed to thermal heating and enhanced mixing processes in the boundary layer, which make it more extended during the months of the warm season.

The analysis of wind direction, on the other hand, highlights the dominant influence of regional circulation patterns and local topographical effects such as that of the katabatic winds or the land breezes, which flow from the mountainous areas towards Limassol during the nighttime hours and resulting in northerly winds, whereas during the hours of sunshine the opposite effect, that of sea breeze is observed, that makes the winds flow from the sea towards the city, resulting in southerly winds and thus contributing to a cooling effect, especially during the hot summer days, and to an improved air quality as it helps reduce the urban pollution as well. Notably, the same wind patterns are observed in the cold and warm seasons at the lowermost altitudes as during night-time northerlies prevail, whereas around sunrise the wind shifts to easterly-southeasterly then to southerlies before changing to southwesterly-westerly and then back to northerlies, with those patterns being more pronounced during the warm six-month period.

Even though the data used here are not extensive enough to classify it as a climatological study, the results still offer valuable insight into the temporal and vertical variability of the wind regimes at Limassol. Moreover, the significance of this study rests in the fact that, for the first time, an analysis like this one is able to be conducted with data acquired by a Doppler lidar – an instrument that is able to extract the information of the wind with both high accuracy and high resolution.

ACKNOWLEDGEMENTS

The study is supported by the ‘EXCELSIOR’: ERATOSTHENES: EXcellence Research Centre for Earth Surveillance and Space-Based Monitoring of the Environment H2020 Widespread Teaming project (www.excelsior2020.eu). The ‘EXCELSIOR’ project has received funding from the European Union’s Horizon 2020 research and innovation programme under Grant Agreement No 857510, from the Government of the Republic of Cyprus through the Directorate General for the European Programmes, Coordination and Development and the Cyprus University of Technology. The authors acknowledge the ATARRI project funded by the European Union’s Horizon Europe Twinning Call (HORIZON-WIDERA-2023-ACCESS-02) under the grant agreement No 101160258.

REFERENCES

[1] C. D. Ahrens and R. Henson, “Earth and Its Atmosphere,” in Meteorology Today,12th Edition, 12th ed., Cengage Learning, 2018, ch. 1, pp. 3–29.
[2] C. D. Ahrens and R. Henson, “Air Pressure and Winds,” in Meteorology Today,12th Edition, 12th ed., Cengage Learning, 2018, ch. 8, pp. 197–225.
[3] W. Jia and X. Zhang, “The role of the planetary boundary layer parameterization schemes on the meteorological and aerosol pollution simulations: A review,” Jul. 15, 2020, Elsevier Ltd. doi: 10.1016/j.atmosres.2020.104890.
[4] Y. Shi, F. Hu, Z. Xiao, G. Fan, and Z. Zhang, “Comparison of four different types of planetary boundary layer heights during a haze episode in Beijing,” Science of The Total Environment, vol. 711, p. 134928, Apr. 2020, doi: 10.1016/j.scitotenv.2019.134928.
[5] G. De Arruda Moreira et al., “Analyzing the turbulent planetary boundary layer by remote sensing systems: The Doppler wind lidar, aerosol elastic lidar and microwave radiometer,” Atmos Chem Phys, vol. 19, no. 2, pp. 1263–1280, Jan. 2019, doi: 10.5194/acp-19-1263-2019.
[6] M. C. Peel, B. L. Finlayson, and T. A. Mcmahon, “Updated world map of the Köppen-Geiger climate classification,” Hydrol. Earth Syst. Sci, vol. 11, pp. 1633–1644, 2007, [Online]. Available: www.hydrol-earth-syst-sci.net/11/1633/2007/

[7] J. H. Schween, A. Hirsikko, U. Löhnert, and S. Crewell, “Mixing-layer height retrieval with ceilometer and Doppler lidar: From case studies to long-term assessment,” Atmos Meas Tech, vol. 7, no. 11, pp. 3685–3704, Nov. 2014, doi: 10.5194/amt-7-3685-2014.
[8] N. J. Harvey, R. J. Hogan, and H. F. Dacre, “A method to diagnose boundary-layer type using doppler lidar,” Quarterly Journal of the Royal Meteorological Society, vol. 139, no. 676, pp. 1681–1693, Oct. 2013, doi: 10.1002/qj.2068.
[9] C. Werner, “Doppler Wind Lidar,” in Lidar: range-resolved optical remote sensing of the atmosphere, New York: NY: Springer New York, 2005, ch. 12, pp. 325–354.
[10] V. Vakkari, E. J. O’Connor, A. Nisantzi, R. E. Mamouri, and D. G. Hadjimitsis, “Low-level mixing height detection in coastal locations with a scanning Doppler lidar,” Atmos Meas Tech, vol. 8, no. 4, pp. 1875–1885, Apr. 2015, doi: 10.5194/amt-8-1875-2015.
[11] F. Kekkou, T. Economou, G. Lazoglou, and C. Anagnostopoulou, “Temperature extremes and human health in Cyprus: Investigating the impact of heat and cold waves,” Environ Int, vol. 199, p. 109451, May 2025, doi: 10.1016/j.envint.2025.109451.